

Simplified Deadbeat Predictive Torque Control Based on Discrete Space Vector Modulation for Driving an Open-End Winding Permanent Magnet Synchronous Motor

Hyung-Woo Lee^{*} Non-member, Jun-Ho Hwang^{**} Non-member
Kyo-Beum Lee^{*a)} Non-member

(Manuscript received Aug. 24, 2023, revised Dec. 5, 2023)
J-STAGE Advance published date : Jan. 26, 2024

This study proposes a simplified deadbeat (DB) predictive torque control (PTC) strategy for driving an open-end winding permanent magnet synchronous motor (OEW-PMSM) to reduce the torque and current ripple. The torque and current ripple are large because the conventional finite set PTC (FS-PTC) uses only one voltage vector in the sampling period. To avoid these problems, a simplified PTC strategy based on discrete space vector modulation (DSVM) is proposed to split the voltage vector into a virtual voltage vector and select the optimal voltage vector. Furthermore, the DB method is used to estimate the reference voltage angle and to thereby select an area that includes the candidate voltage vectors to reduce the computational burden. Among these candidate voltage vectors in the selected area, the optimal voltage vector can be selected by calculating the cost function. Therefore, one or more voltage vectors are used in the sampling period, reducing the torque and current ripple. The effectiveness of the proposed strategy is verified through simulation and experimental results.

Keywords: open-end winding permanent magnet synchronous motor (OEW-PMSM), dual inverter, predictive torque control (PTC)

1. Introduction

Interior permanent magnet synchronous motors (IPMSMs) have attracted much industrial interest owing to their superior efficiency and high power density. Recently, IPMSMs with a modified mechanical structure have been introduced to achieve high performance, specifically, high speed and power quality. In this regard, studies are actively investigating open-end winding (OEW) motors, in which the neutral point of the stator winding is separated. Thus, an OEW motor fed by a dual inverter has a structure for applying a voltage to both ends of the stator winding^{(1)–(5)}. The dual inverter consists of double two-level inverters. It generates high voltages at the stator winding and affords advantages such as the multilevel effect of phase voltages and fault tolerance. Additionally, unlike other three-level inverters, it does not contain clamping diodes, and therefore, neutral point control is not required. Therefore, studies have focused on dual inverters for driving OEW motors^{(6)–(15)}.

Various advanced control techniques have been developed to deal with the increased processing and performance capabilities of microprocessors. One such technique is the finite-set model predictive control (FS-MPC) method that is based

on a mathematical model of the load⁽¹⁶⁾⁽¹⁷⁾. This method is used in various power conversion systems owing to its intuitive concept and fast response. Additionally, this method can also be used to control the motor by using the model of the torque and stator magnetic flux; this is called the finite-set predictive torque control (FS-PTC) method. The conventional FS-PTC (C-PTC) method predicts the future states based on the available voltage vectors and determines the optimal switching state by cost function optimization. The C-PTC method only uses fixed real voltage vectors for constructing the candidate voltage vectors to calculate the cost function. Thus, it can obtain a fast response in the transient owing to the optimal state in one sampling period^{(18)–(20)}. However, when applying the C-PTC method, the ripple component of the torque and magnetic flux are large in the steady state. Because this method only considers a few candidate voltage vectors that consist of the fixed real voltage vectors according to the switching states, the cost function cannot be calculated precisely. Additionally, the single switching state in one sampling period results in a large torque and magnetic flux ripple with the current ripple, and this degrades the control performance.

To reduce the current ripple by reducing the harmonics, a PTC method based on discrete space vector modulation (DSVM) has been introduced. Unlike the C-PTC method, DSVM-based PTC uses more candidate voltage vectors for calculating the cost function by generating virtual voltage vectors. The virtual voltage vectors can be constructed by splitting the real voltage vectors in the space vector diagram^{(21)–(23)}. Therefore, the optimal candidate voltage vector

a) Correspondence to: Kyo-Beum Lee. E-mail: kyl@ajou.ac.kr
^{*} Department of Electrical and Computer Engineering, Ajou University
206, World-cup ro, Yeongtong-gu, Suwon-si, Gyeonggi-do, South Korea
^{**} Department of H&A Power Conversion, LG Electronics Inc.
51, Gasan digital 1-ro, Geumcheon-gu, Seoul, South Korea

that minimizes the cost function can be selected and modulated for the switching operation through a comparison with the carrier. Compared with the C-PTC method, the DSVM-based PTC method applies various switching states that include not only effective but also zero voltage vectors in one sampling period⁽²⁴⁾⁽²⁵⁾. Thus, the DSVM-based PTC method can improve the precision of the calculation of the cost function, resulting in a reduction in the torque and magnetic flux ripple. Further, because of the comparison and switching operation between the selected voltage vector and carrier, the fixed switching frequency can be guaranteed. Various studies have investigated the implementation of the DSVM strategy to generate a virtual voltage vector. The virtual voltage vectors were synthesized using an offline table based on real voltage vectors⁽²⁶⁾. This approach is intuitive; however, the computational burden of the synthesizing process is large. In previous study, virtual voltage vectors were synthesized based on the interval of the prefixed sampling period⁽²⁷⁾. However, the main drawback of the DSVM-based PTC method is the large computational burden caused by numerous candidate voltage vectors for calculating the cost function.

Because the C-PTC method predicts all the switching states, the computational burden is a fatal obstacle for conducting the control algorithm. The main cause of the increased computational burden is the adoption of a multilevel topology that has numerous power switch devices. Further, the numerous candidate voltage vectors caused by the use of the DSVM strategy increase the computational burden of the microprocessor that runs the control algorithm. Consequently, a microprocessor having higher performance is required, and therefore, the cost of the system configuration increases. To overcome this issue, various deadbeat (DB) methods have been studied. For example, the DB torque and flux control (DB-DTFC) based on the inverse-model-based solution using the torque equation was proposed⁽²⁸⁾. Further, based on the concept of the nearest voltage point (NVP), the optimal dynamic trajectory was produced online⁽²⁹⁾. This technique has good performance but a complex implementation. A grid-connected system was applied to estimate the reference voltage angle by using a mathematical model of grid voltages⁽³⁰⁾⁽³¹⁾.

This study proposed a simplified DB-PTC method for driving OEW-PMSMs to reduce the torque and magnetic flux ripple. This method uses DSVM to select the optimal real and virtual reference voltage vectors. As the number of virtual voltage vectors increases, more candidate voltage vectors can be considered for cost function optimization. However, considering the number of candidate voltage vectors within a limited sampling period, the computational burden is increased. To avoid this computational burden, the location of the reference voltage should be estimated to select a specific area that includes the reference candidate voltage vectors. The real-time location of the reference voltage can be estimated precisely by using the mathematical voltage model of the OEW-PMSM. From the candidate voltage vectors in the selected area, the cost function can be calculated and optimized, resulting in the selection of the optimal reference voltage vector. Subsequently, the selected optimal voltage vector is modulated for comparison with the carrier and for determining the switching state of the dual inverter. Because one

or more voltage vectors including the zero voltage vector are applied in one sampling period, the torque and magnetic flux ripple can be reduced compared to those in the C-PTC. The effectiveness of the proposed DVSM-based DB-PTC method is verified through a simulation and experimental results.

2. Mathematical Model of OEW-PMSM Fed by Dual Inverter

2.1 Modeling of Dual Inverter Fig. 1 shows a circuit diagram of an OEW-IPMSM fed by a dual inverter with isolated dc-sources. The dual inverter consists of double two-level inverters. Each inverter is connected to dc-sources that are isolated from each other. Therefore, in contrast to a single inverter, the three-phase voltage at the stator winding is generated by the combination of the output phase voltages of inverters 1 and 2. The three-phase voltages derived by the switching states of each inverter can be expressed as follows:

$$\begin{bmatrix} u_{as(n)} \\ u_{bs(n)} \\ u_{cs(n)} \end{bmatrix} = \begin{bmatrix} V_{dc(n)}/3 \cdot (2S_{a(n)} - S_{b(n)} - S_{c(n)}) \\ V_{dc(n)}/3 \cdot (2S_{b(n)} - S_{c(n)} - S_{a(n)}) \\ V_{dc(n)}/3 \cdot (2S_{c(n)} - S_{a(n)} - S_{b(n)}) \end{bmatrix} \dots \dots \dots (1)$$

where $u_{as(n)}$, $u_{bs(n)}$, and $u_{cs(n)}$ are the three phase voltages of each inverter; n takes a value of 1 or 2 to indicate inverter 1 or 2, respectively; $V_{dc(n)}$ indicates the dc-link voltage; and $S_{a(n)}$, $S_{b(n)}$, and $S_{c(n)}$ indicate the switching states of each inverter, respectively. According to the output phase voltage determined by the switching states of inverter 1 and 2, the three-phase voltage of the dual inverter can be represented as

$$\begin{bmatrix} u_{as} \\ u_{bs} \\ u_{cs} \end{bmatrix} = \begin{bmatrix} u_{as(1)} - u_{as(2)} \\ u_{bs(1)} - u_{bs(2)} \\ u_{cs(1)} - u_{cs(2)} \end{bmatrix} \dots \dots \dots (2)$$

where u_{as} , u_{bs} , and u_{cs} are the output three-phase voltages of the dual inverter, and they are equal to the three-phase voltages of the stator winding of the OEW-PMSM. From the

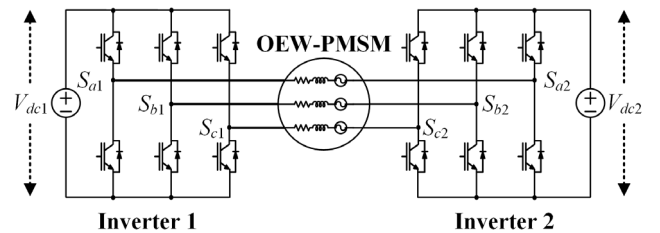


Fig. 1. Circuit diagram of OEW-IPMSM fed by dual inverter

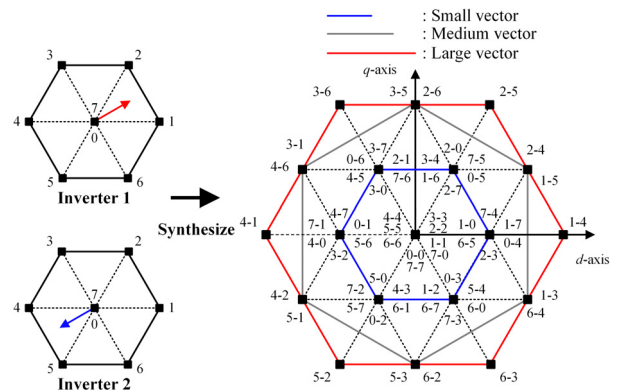


Fig. 2. Synthesized voltage vector diagram of dual inverter

three-phase voltages determined by the switching state, the synthesized voltage vector diagram of the dual inverter is represented as shown in Fig. 2. The voltage vectors of the dual inverter can be equalized to 19 voltage vectors considering the magnitude and phase determined by the switching states of inverters 1 and 2.

From (1) and (2), the three-phase voltages of the stator windings generated by the dual inverter are boosted compared to those of the single inverter. Further, a multilevel effect appears owing to the synthesized voltage vector of the dual inverter caused by the increasing number of switching states.

2.2 Continuous Model of OEW-PMSM By applying the Park transformation to the three-phase voltages of stator windings, the continuous d - q axis synchronous coordinate voltages of IPMSM can be obtained as follows:

$$\begin{bmatrix} u_d \\ u_q \end{bmatrix} = \begin{bmatrix} R_s i_d + \frac{d}{dt} \lambda_d - \omega_r L_q i_q \\ R_s i_q + \frac{d}{dt} \lambda_q + \omega_r L_d i_d + \omega_r \lambda_f \end{bmatrix} \dots \dots \dots (3)$$

where u_d and u_q are the d - q axis voltages of the stator winding, i_d and i_q are the d - q axis stator currents, R_s is the stator resistance, L_d and L_q are the d - q axis stator inductances, λ_d and λ_q are the d - q axis stator flux, ω_r is the angular frequency, and λ_f is the permanent magnet flux linkage of the motor. The electromagnetic torque can be expressed as follows:

$$T_e = \frac{3}{2} P_n ((L_d - L_q) i_d i_q + \lambda_f i_q) \dots \dots \dots (4)$$

where T_e is the electromagnetic torque and P_n , the pole pair of OEW-IPMSM.

3. Conventional FS-PTC Strategy

3.1 Discrete Modeling of OEW-PMSM The dynamic model of the IPMSM in the stationary reference frame can be discretized based on the continuous model. When Euler's discretization is applied, the prediction model of the stator current can be expressed as

$$\begin{aligned} i_d(k+1) &= (1 - R_s T_s / L_d) i_d(k) + L_q T_s \omega_r(k) / L_d i_q(k) \\ &\quad + T_s / L_d \cdot u_d(k) \\ i_q(k+1) &= (1 - R_s T_s / L_q) i_q(k) - L_d T_s \omega_r(k) / L_q i_d(k) \\ &\quad + T_s / L_q \cdot u_q(k) - \lambda_f T_s \omega_r(k) / L_q \dots \dots \dots (5) \end{aligned}$$

where (k) and $(k+1)$ are the present and prediction sampling discrete steps, T_s is the sampling period, $u_d(k)$ and $u_q(k)$ are the (k) th d - q axis reference voltages, and $\omega_r(k)$ is the (k) th angular speed. From the predicted current model, the prediction model of the stator flux can be described as follows:

$$\lambda_s(k+1) = \sqrt{(L_d i_d(k+1) + \lambda_f)^2 + (L_q i_q(k+1))^2} \dots \dots \dots (6)$$

From the derived prediction model of the current and stator flux, the prediction model of electromagnetic torque can be expressed as follows:

$$\begin{aligned} T_e(k+1) &= \frac{3}{2} P_n \{ \lambda_s(k+1) \cdot i_q(k+1) \\ &\quad + (L_d - L_q) i_d(k+1) i_q(k+1) \} \dots \dots \dots (7) \end{aligned}$$

3.2 Cost Function Construction After deriving the

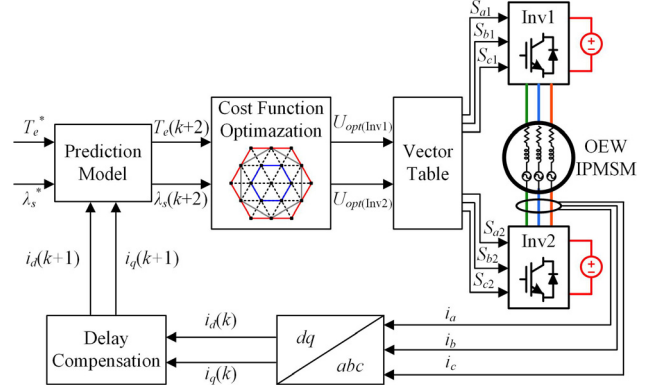


Fig. 3. Control block of conventional C-PTC

prediction model, the cost function can be constructed as follows:

$$g = W_\lambda \cdot |\lambda_s^* - \lambda_s(k+1)| + W_T \cdot |T_e^* - T_e(k+1)| \dots \dots \dots (8)$$

where λ_s^* is the reference stator flux, T_e^* is the reference torque, and W_λ and W_T are the weighing factors of the stator flux and torque, respectively.

3.3 Control Sequence of C-PTC Method Fig. 3 shows the control block diagram of the C-PTC method. By using the sensed three-phase current and angular speed, the prediction model of the stator flux and torque can be derived by (5) to (7). The cost function is constructed using the predicted models with the reference value of the stator flux and torque. Then, the cost function can be optimized through an iterative computation based on the available switching states. The candidate voltage vectors that used in cost function are the 19 switching states in Fig. 2. The cost function is calculated for the voltage vector corresponding to each switching state. The one of 19 voltage vectors with the minimum output of the cost function is selected as the final switching state of the next sampling period⁽³⁰⁾⁽³¹⁾. Because the C-PTC method uses the single zero or real voltage vector in one sampling period, the magnitude of the torque and flux ripple are increased compared to the case of using DSVM.

4. Proposed FS-PTC Strategy Using Simplified Deadbeat Method

4.1 DSVM-based PTC Method Because the C-PTC method uses only the real voltage vector in one sampling period, the ripple of the torque and stator flux is large in the steady state. By splitting the real voltage vector of the dual inverter into the virtual voltage vector, the switching states can be optimized owing to the subdivided virtual voltage vectors. Fig. 4 shows the subdivided voltage vector diagram of the dual inverter based on DSVM. The synthesized voltage vector diagram is subdivided into 12 sectors according to the location of the reference voltage vector. The virtual voltage vector is generated symmetrically with respect to the d - and q -axes. The number of virtual voltage vectors in each sector is the same and is determined by the number of subdivisions. The total number of voltage vectors according to the constant of subdivision (T) can be defined as follows:

$$T(n) = 6n^2 + 6n + 1 \dots \dots \dots (9)$$

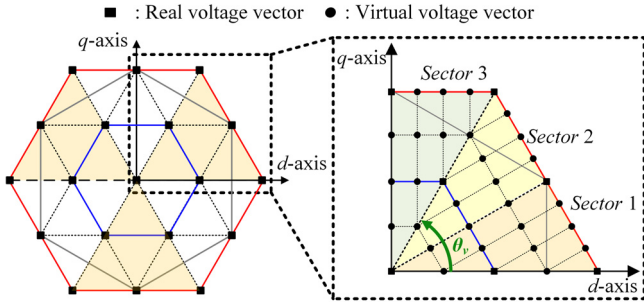


Fig. 4. Subdivided voltage vector diagram of dual inverter based on DSVM

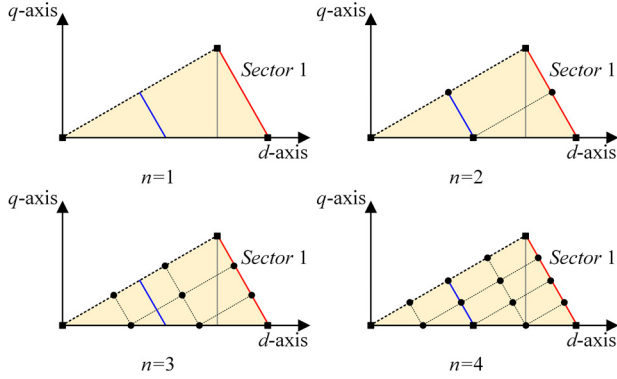


Fig. 5. DSVM according to constant of subdivision

where n represents the constant of subdivisions. Depending on the constant of subdivision, the number of candidate voltage vectors is determined. Fig. 5 shows the DSVM according to the constant of subdivision at sector 1. As the number of subdivisions increases, the ideal voltage vector can be selected; however, the computational burden also increases. Thus, the constant of subdivision should be selected in consideration of the computational burden.

After the selection of the sector, the stationary reference d - q axis candidate voltage vectors in the selected sector can be generated using the constant of subdivision and can be expressed as follows:

$$\begin{bmatrix} v_d^* \\ v_q^* \end{bmatrix} = \begin{bmatrix} \frac{V_{dc1} + V_{dc2}}{6n} ((a + 2e)x + 3by) \\ \frac{\sqrt{3}(V_{dc1} + V_{dc2})}{6n} ((cx + (d + 2f)y)) \end{bmatrix} \dots (10)$$

where x and y represent the d - q axis coordinate. After the sector is determined from the reference voltage angle, the coefficient can be defined as shown in Table 1.

If all voltage vectors are considered to calculate the cost function, the computational burden becomes large. To avoid this issue, the cost function should be calculated based on the specific candidate voltage vectors included in the selected sector.

4.2 Estimation of Reference Voltage Vector Location for DB To determine the sector in which the reference voltage angle is located, the voltage angle estimation must be accurate. This study estimates the voltage angle using the model parameter. The d - q axis reference voltage at the synchronous frame can be expressed as follows:

$$u_{de_est}^* = (L_d/T_s) \cdot i_d(k+1) + (R_s - L_q/T_s) \cdot i_d(k+1)$$

Table 1. Coefficient according to sector

Sector	a	b	c	d	e	f
1	1	1	-1	1	0	0
2	-1	1	1	1	0	0
3	0	0	0	0	1	1
4	0	0	0	0	-1	1
5	1	-1	1	1	0	0
6	-1	-1	-1	1	0	0
7	-1	-1	1	-1	0	0
8	1	-1	-1	-1	0	0
9	0	0	0	0	-1	-1
10	0	0	0	0	1	-1
11	-1	1	-1	-1	0	0
12	1	1	1	-1	0	0

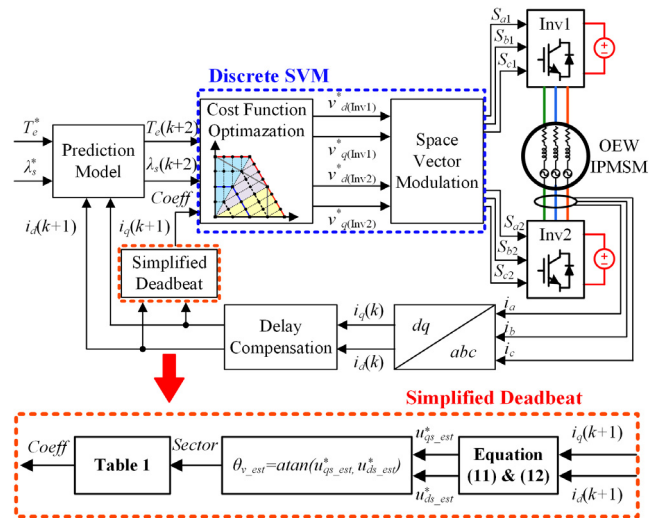


Fig. 6. Control block diagram of proposed simplified DB-PTC method

$$\begin{aligned} & -\omega_r L_d \cdot i_q(k+1) \\ u_{qe_est}^* &= (L_q/T_s) \cdot i_q(k+1) + (R_s - L_d/T_s) \cdot i_q(k+1) \\ & + \omega_r L_d \cdot i_d(k+1) + \omega_r \lambda_f \dots (11) \end{aligned}$$

After the estimation of the d - q axis reference voltage at the synchronous frame, the reference voltage can be estimated by the inverse Park Transformation, and it is derived as follows:

$$\begin{bmatrix} u_{ds_est}^*(k+1) \\ u_{qs_est}^*(k+1) \end{bmatrix} = \begin{bmatrix} \cos \theta_r & -\sin \theta_r \\ \sin \theta_r & \cos \theta_r \end{bmatrix} \begin{bmatrix} u_{de_est}^*(k+1) \\ u_{qe_est}^*(k+1) \end{bmatrix} \dots (12)$$

The reference voltage angle can be defined by the stationary frame d - q axis voltage, and it is expressed as follows:

$$\theta_{v_est}^* = \text{atan} \left(\frac{u_{qs_est}^*}{u_{ds_est}^*} \right) \dots (13)$$

By using the estimated reference voltages, the reference voltage angle and location of the reference voltage vector can be estimated.

4.3 Control Sequence of Proposed Simplified DB-PTC Method Fig. 6 shows the control block diagram of the proposed simplified DB-PTC method. By using the predicted current model and parameter of the OEW-PMSM, the

location of the reference voltage vector can be estimated, and consequently, the coefficient can be selected. By using this proposed method, the computational burden can be reduced by estimating and selecting the location of the reference voltage vector. After optimizing the cost function based on the DSVM, the reference voltage can be determined. Finally, the switching states of the dual inverter can be determined by comparing the reference voltage with the carrier. Therefore, the effective voltage vector as well as the zero voltage vector can be considered within one sampling period. The proposed method uses DSVM to apply more subdivided candidate vector compared to the C-PTC, A drawback of the C-PTC is complimented such as large ripple in stator current. In addition, sufficient constant of subdivisions n enables similar or better performance compared to SVPWM, but this requires consideration of the amount of computation over the increased the constant of subdivisions.

5. Simulation Results

The proposed DVSM-based DB-PTC method was verified using a simulation model. Table 2 lists the simulation parameters of the OEW-IPMSM. The sampling period was set to $50\mu\text{s}$, and the switching frequency was set to 20 kHz. The dc-link voltage of both inverters 1 and 2 was 80 V, and it was supplied by isolated DC power sources. The weighting factors of the torque and flux, consisting of the cost function, were set to 1 and 200, respectively. In the process of setting the weighting factor for torque and flux, the initial value was set in proportion to the rating of each parameter. This allowed the two parameters to be reflected at a similar rate in the cost function, and then the weighting factor values corresponding to each parameter were changed empirically to achieve optimal performance. Therefore, the weighting factors of each parameter applied in the simulation and experiment have different values depending on the difference between the ideal and actual conditions. Additionally, considering the performance of the microprocessor and the computational burden, n was set to 4. To verify the proposed method, the conventional and proposed methods were simulated under the same condition.

Fig. 7 shows the simulation results of the a -phase pole voltage when C-PTC method and the proposed method applied at 500 rpm. In Fig. 7, v_{ap1} , v_{ap2} , T_s represent pole voltage of inverter 1, inverter 2, and sampling period, respectively. In C-PTC method, only one voltage vector selected by cost function is applied during sampling period. Therefore, the

pole voltages of the dual inverter remain the same state during one sampling period. In the proposed DB-PTC method, the reference voltage vector is applied by DSVM scheme. Since the reference voltage vector is applied in the same way as SVPWM within one sampling period, the polar voltage of the dual inverter appears in a symmetrical form using zero voltage vectors within the sampling period. This fundamental difference in the way reference voltage vector is applied, causes the proposed DB-PTC method to reduce current ripple compared to the C-PTC method.

Fig. 8 shows the simulation results of torque control when the C-PTC method and proposed DB-PTC method are applied at 500 rpm. Before 0.4 s, the reference torque was 20% of the rated torque, and after 0.4 s, the reference torque changed to 60% of the rated torque. Furthermore, the reference flux was maintained at 0.1133 Wb. From Fig. 8(a), by using the C-PTC method, the total harmonic distortion (THD) of the phase current was 26.81% and 9.87% at each torque reference condition. However, when the proposed

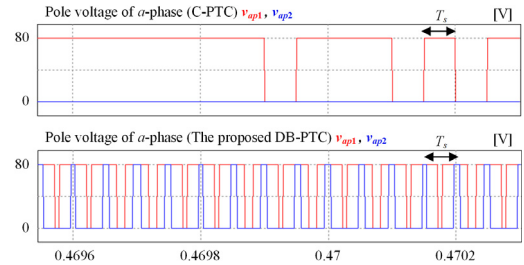
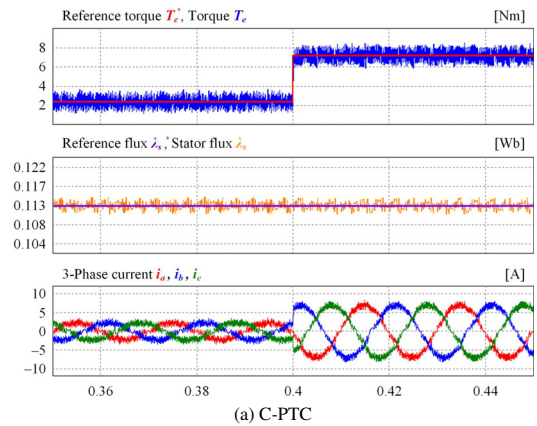
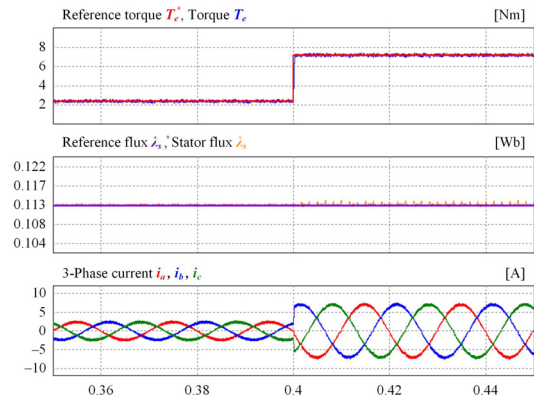


Fig. 7. Simulation results of a-phase pole voltage



(a) C-PTC



(b) The proposed DB-PTC

Fig. 8. Simulation results of torque control at 500 rpm

Table 2. OEW-PMSM parameters

Parameters	Value	Unit
Rated power	2.2	kW
Rated speed (N_{r_rated})	-1750	rpm
Rated torque (T_{e_rated})	12	Nm
Stator resistance (R_s)	0.213	Ω
d -axis inductance (L_d)	1.60	mH
q -axis inductance (L_q)	2.18	mH
Permanent magnet flux (ϕ_f)	0.1133	Wb
Number of poles (P)	12	

DB-PTC method was applied, the THD of the current reduced to 7.07% and 3.44%.

Fig. 9(a) and (b) show the simulation results of torque control at 800 rpm. When the C-PTC method was applied, the THD of the current was 28.9% and 9.32%. By contrast, when using the DVSM-based DB-PTC method, the THD of the current reduced to 8.11% and 3.48%. These simulation results indicate that when the proposed method is applied, the current ripple was reduced. Fig. 10 shows the analysis diagram of the THD of the current. The THD of the current varies according to the load torque, rotor speed, and constant of subdivision. For the same n , the THD of the current decreases as the load torque increases or rotor speed decreases. In addition, as n increased, the THD of the current was superior owing to the increase in the selectable candidate voltage

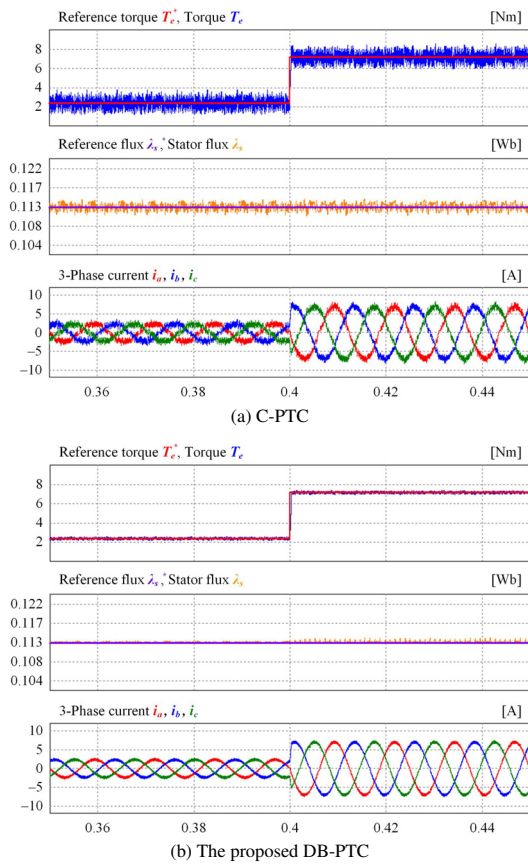


Fig. 9. Simulation results of torque control at 800 rpm

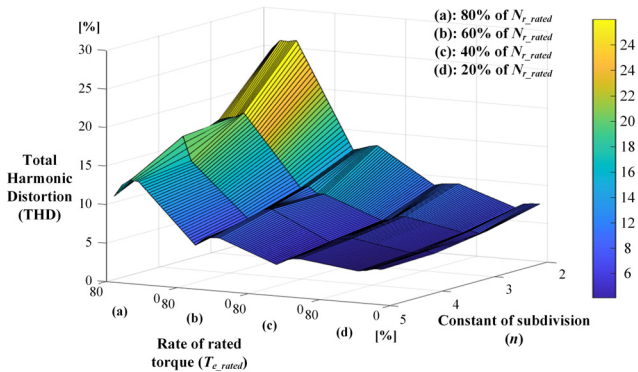


Fig. 10. Analysis diagram of current THD according to torque, rotor speed, and constant of subdivision

vectors. In PWM techniques, as the fundamental frequency of the motor increases, the THD also increases. The proposed method also has the same tendency because the selected reference voltage vector is applied using the DSVM. Therefore, the proposed method also tends to increase THD at higher speeds, resulting in low THD at lower speeds. In addition, the effect of reducing THD by increasing n is basically more pronounced in high-speed region with high THD.

6. Experimental Results

The validity and performance of the proposed DVSM-based DB-PTC method have been experimentally investigated. The experimental conditions and parameters of the OEW-IPMSM are identical to the simulation parameter as presented in Table 2. Fig. 11 shows the developed experimental hardware setup for investigating the feasibility of the proposed method. It comprised a dual inverter with insulated-gate bipolar transistor (IGBT) power modules and a DSP control board. A TMS320F28377S microprocessor was used for implementing the software algorithm. To load the machine, an induction motor coupled to the OEW-IPMSM was controlled by YASKAWA. The C-PTC and proposed DB-PTC methods were performed on the same experimental setup for comparison under the same sampling time of $50 \mu\text{s}$. Moreover, the weighing factors of the flux and torque were experimentally tuned to 0.3 and 200, respectively.

Fig. 12 shows the experimental waveform of the stationary d - q axis reference voltage. After the reference voltage angle is estimated by (13), the sector can be obtained. The coefficient is determined from the sector, as shown in Table 1. As a result, the stationary d - q reference voltage can be generated.

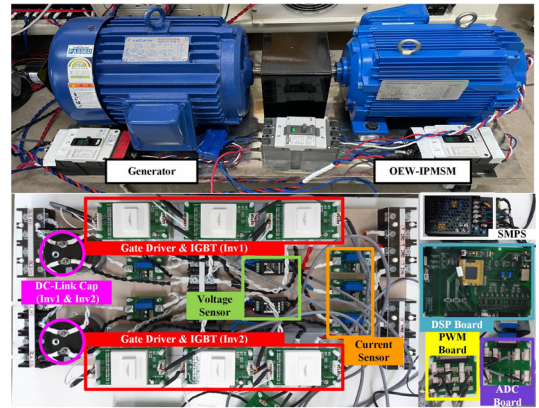


Fig. 11. Developed experimental setup of dual inverter for driving OEW-PMSM

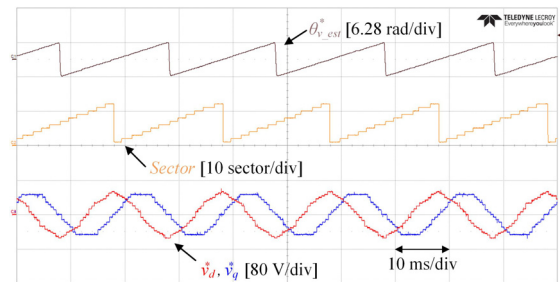
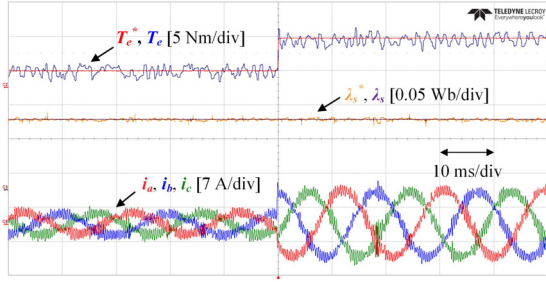
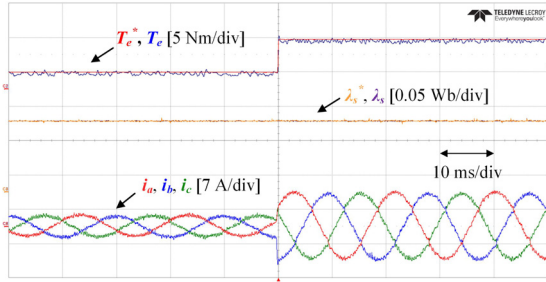


Fig. 12. Sector according to the estimated reference voltage angle and stationary d - q axis reference voltage

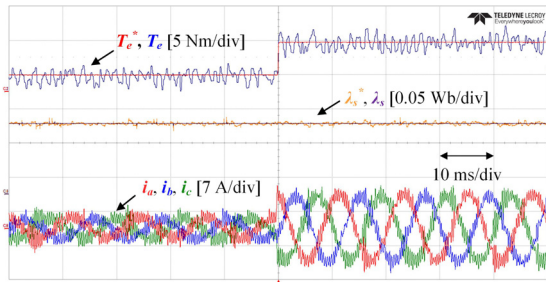


(a) C-PTC

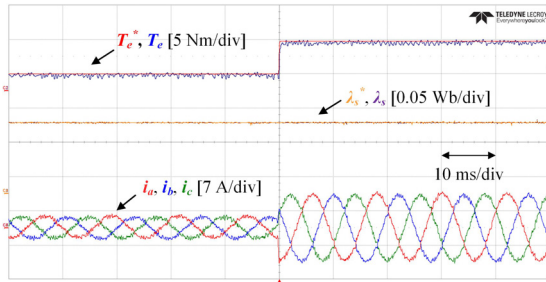


(b) The proposed DB-PTC

Fig. 13. Experimental results of the torque control at 500 rpm



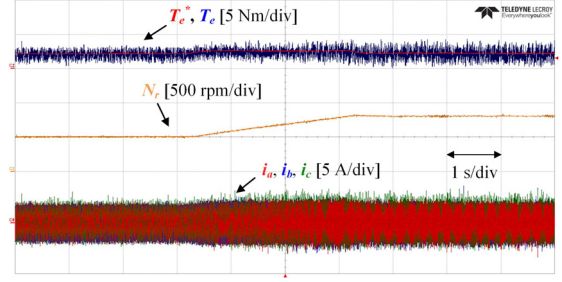
(a) C-PTC



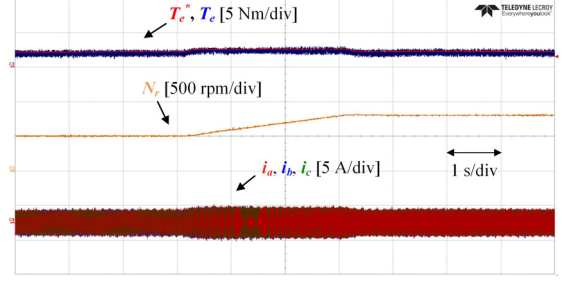
(b) The proposed DB-PTC

Fig. 14. Experimental results of torque control at 800 rpm

Fig. 13(a) and (b) shows the experimental results of torque control when the C-PTC and proposed DVSM-based DB-PTC method are applied at 500 rpm. The reference torque was changed from 20% of the rated torque to 60% of the rated torque. Further, the magnitude of the reference flux was set at 0.1133 Wb. The peak-to-peak torque value that represents the torque ripple was reduced from 3.1 Nm to 0.8 Nm when the C-PTC and proposed DVSM-based DB-PTC method were applied, respectively. Fig. 14(a) and (b) shows the experimental results of torque control at 800 rpm. When the proposed method was applied, the peak-to-peak value of torque ripple reduced from 4.4 Nm to 1.1 Nm. The experimental results shown in Figs. 13 and 14 confirmed that the torque and

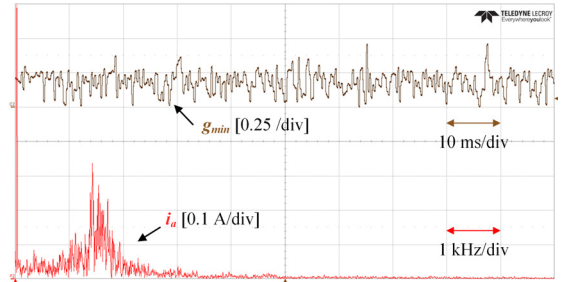


(a) C-PTC

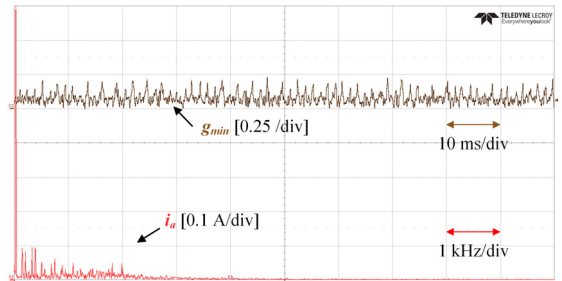


(b) The proposed DB-PTC

Fig. 15. Experimental results of speed control



(a) C-PTC



(b) The proposed DB-PTC

 Fig. 16. Minimum value of cost function and harmonic spectrum results of a -phase current

current ripple improved when the proposed method was applied.

Fig. 15 shows the experimental results when the speed controller was applied. The rotor speed was controlled from 500 rpm to 800 rpm, and the load torque of OEW-PMSM was set to 20% of the rated torque. When the proposed DVSM-based DB-PTC method was applied, the torque and current ripple improved compared to those in the C-PTC method. Further, in a transient state with increasing rotor speed, the stability of control was also improved.

Fig. 16(a) and (b) respectively show the experimental results including the minimum value of the cost function (g_{min}) and a -phase current's harmonic spectrum when the C-PTC and proposed DVSM-based DB-PTC method were applied.

As shown in Fig. 16, when using the proposed method, the minimum value of the cost function was lower than that with the C-PTC method. This represents that the error of the torque and flux between the reference and output values decreased when the proposed method was applied. In addition, the harmonic components of the a -phase current at low frequencies of under approximately 5 kHz were reduced. When using the C-PTC method, the peak value of the harmonic component was approximately 0.35 A at around 2 kHz. By contrast, when using the proposed method, the peak value of the harmonic component reduced to under 0.1 A. The experimental results and analysis indicate that when using the proposed DB-PTC method, the torque and flux ripple were improved compared to those with the C-PTC method, and the feasibility of the proposed method was verified.

7. Conclusion

This study proposed a simplified DB-PTC method for driving OEW-PMSMs to improve the stability in the steady state. By using the mathematical parameters of the OEW-PMSM, the location of the reference voltage vector was estimated, and the section could be selected. Thus, the implementation of the proposed DB-PTC was simple and accessible, because the stator voltage model was used for estimating the angle of the reference voltage. Cost function optimization was performed using the candidate voltage vectors in the selected section. As a result, the torque and current ripple were reduced by using the optimal voltage vector in the subdivided candidate voltage vectors. The voltage vector was subdivided considering the computational burden of the microprocessor. Further, the delay compensation in the proposed DB-PTC method was considered sufficient. The effectiveness and feasibility of the proposed simplified DVSM-based DB-PTC methods were verified through the simulation and experimental results.

Acknowledgement

This work was supported in part by the Korea Institute of Energy Technology Evaluation and Planning (KETEP) and the Ministry of Trade, Industry & Energy (MOTIE) of the Republic of Korea under Grant 2022550000110.

References

- (1) M. Tursini, E. Chiricozzi, and R. Petrella: "Feedforward flux-weakening control of surface-mounted permanent-magnet synchronous motors accounting for resistive voltage drop", *IEEE Trans. Power Electron.*, Vol.57, No.1, pp.440–448 (2010)
- (2) S. Kim and J.-K. Seok: "Maximum voltage utilization of IPMSMs using modulating voltage scalability for automotive applications", *IEEE Trans. Power Electron.*, Vol.28, No.12, pp.5639–5646 (2013)
- (3) Q. An, J. Liu, L. Sun, and L. Sun: "Dual-space vector control of open-end winding permanent magnet synchronous motor drive fed by dual inverter", *IEEE Trans. Power Electron.*, Vol.31, No.12, pp.8329–8342 (2016)
- (4) V.T. Somasekhar, S. Srinivas, and K.K. Kumar: "Effect of zero-vector placement in a dual-inverter fed open-end winding induction-motor drive with a decoupled space-vector PWM strategy", *IEEE Trans. Power Electron.*, Vol.55, No.6, pp.2497–2505 (2008)
- (5) P. Sandulescu, F. Meiguet, X. Kestelyn, E. Semail, and A. Bruyère: "Control strategies for open-end winding drives operating in the flux-weakening region", *IEEE Trans. Power Electron.*, Vol.29, No.9, pp.4829–4842 (2014)
- (6) Y. Lee and J.-I. Ha: "Hybrid modulation of dual inverter for open-end permanent magnet synchronous motor", *IEEE Trans. Power Electron.*, Vol.30, No.6, pp.3286–3299 (2015)
- (7) A. Mizukoshi and H. Haga: "Reduction of voltage harmonics in an open-end winding induction motor driven by a dual-inverter with a floating capacitor in a partial-load condition", *IEEJ Journal of Industry Applications*, Vol.10, No.5, pp.564–574 (2021)
- (8) T. Kimura, T. Yamada, R. Kazaoka, and T. Noguchi: "Control method of dual inverter system for EV with one battery", *IEEJ Journal of Industry Applications*, Vol.12, No.3, pp.376–383 (2022)
- (9) A. Mizukoshi and H. Haga: "Voltage harmonic analysis of typical PWM strategies in a dual inverter with floating capacitor in the partial-load condition", *IEEJ Journal of Industry Applications*, Vol.11, No.1, pp.163–174 (2021)
- (10) Y. Zuo, X. Zhu, X. Si, and C.H.T. Lee: "Fault-tolerant control for multiple open-leg faults in open-end winding permanent magnet synchronous motor system based on winding reconnection", *IEEE Trans. Power Electron.*, Vol.36, No.5, pp.6068–6078 (2021)
- (11) T. Sakurai and H. Haga: "Power decoupling control of electrolytic capacitorless dual-inverter to reduce interharmonic current under periodic load fluctuation", *IEEJ Journal of Industry Applications*, Vol.12, No.5, pp.990–999 (2023)
- (12) C. Jiang, H. Liu, P. Wheeler, F. Wu, Z. Cai, and J. Huo: "A novel open-circuit fault detection and location for open-end winding PMSM based on differential-mode components", *IEEE Trans. Ind. Electron.*, Vol.69, No.8, pp.7776–7786 (2022)
- (13) T. Sakurai, Y. Ohno, and H. Haga: "Control method of electrolytic capacitorless dual inverter-fed IPMSM under periodic load torque fluctuations", *IEEJ Journal of Industry Applications*, Vol.11, No.6, pp.833–844 (2022)
- (14) R. Menon, N.A. Azeez, A.H. Kadam, S.S. Williamson, and C. Bacioiu: "An instantaneous power balancing technique for an open-end IM drive using carrier-based modulation for vehicular application", *IEEE Trans. Ind. Electron.*, Vol.66, No.12, pp.9217–9225 (2019)
- (15) H.-W. Lee, S.-J. Jang, and K.-B. Lee: "Advanced DPWM method for switching loss reduction in isolated DC type dual inverter with open-end winding IPMSM", *IEEE Access*, Vol.11, pp.2700–2710 (2023)
- (16) Z. Zhou, C. Xia, Yan, Y.Z. Wang, and T. Shi: "Torque ripple minimization of prediction torque control for PMSM with extended control set", *IEEE Trans. Ind. Electron.*, Vol.64, No.9, pp.6930–6939 (2017)
- (17) Y. Araki, K. Abe, K. Ohishi, Y. Yokokura, J. Sano, and K. Kobayashi: "Harmonic current reduction control based on model predictive direct current control of IPMSM and input grid circuit", *IEEJ Journal of Industry Applications*, Vol.9, No.1, pp.17–26 (2019)
- (18) Y. Cho, Y. Bak, and K.-B. Lee: "Torque-ripple reduction and fast torque response strategy for predictive torque control of induction motors", *IEEE Trans. Power Electron.*, Vol.33, No.3, pp.2458–2470 (2018)
- (19) L.A. Adase, I.M. Alsofyani, and K.-B. Lee: "Predictive torque control with simple duty-ratio regulator PMSM for minimizing torque and flux ripples", *IEEE Access*, Vol.8, pp.2373–2381 (2020)
- (20) A.A. Ahmed, B.K. Koh, H.S. Park, K.-B. Lee, and Y.I. Lee: "Finite-control set model predictive control method for torque control of induction motors using a state tracking cost index", *IEEE Trans. Ind. Electron.*, Vol.64, No.3, pp.1916–1928 (2017)
- (21) I.M. Alsofyani and K.-B. Lee: "A unidirectional voltage vector preselection strategy for optimizing model predictive torque control with discrete space vector modulation of IPMSM", *IEEE Trans. Ind. Electron.*, Vol.69, No.12, pp.12305–12315 (2022)
- (22) M. Amiri, J. Milimonfared, and D.A. Khaburi: "Predictive torque control implementation for induction motors based on discrete space vector modulation", *IEEE Trans. Ind. Electron.*, Vol.65, No.9, pp.6881–6889 (2018)
- (23) I. Osman, D. Xiao, M.F. Rahman, M. Norambuena, and J. Rodriguez: "Discrete space vector modulation based model predictive flux control with reduced switching frequency for IM drive", *IEEE Trans. Energy Convers.*, Vol.36, No.2, pp.1357–1367 (2021)
- (24) Y. Zhang, H. Jiang, and H. Yang: "Model predictive control of PMSM drives based on general discrete space vector modulation", *IEEE Trans. Energy Convers.*, Vol.36, No.2, pp.1300–1307 (2021)
- (25) J.-S. Lee, K.-B. Lee, and F. Blaabjerg: "Predictive control with discrete space-vector modulation of Vienna rectifier for driving PMSG of wind turbine systems", *IEEE Trans. Power Electron.*, Vol.34, No.12, pp.12368–12383 (2019)
- (26) Y. Yang, H. Wen, M. Fan, X. Zhang, L. He, R. Chen, M. Xie, M. Norambuena, and J. Rodriguez: "Low complexity finite-control-set MPC based on discrete space vector modulation for T-type three-phase three-level converters", *IEEE Trans. Power Electron.*, Vol.37, No.1, pp.392–403 (2022)
- (27) I. Osman, D. Xiao, K.S. Alam, S.M.S.I. Shakib, M.P. Akter, and M.F. Rahman: "Discrete space vector modulation-based model predictive torque control with no suboptimization", *IEEE Trans. Ind. Electron.*, Vol.67, No.10,

- pp.8164–8174 (2020)
- (28) Y. Wang, X. Wang, W. Xie, F. Wang, M. Dou, R.M. Kennel, R.D. Lorenz, and D. Gerling: “Deadbeat model-predictive torque control with discrete space-vector modulation for PMSM drives”, *IEEE Trans. Ind. Electron.*, Vol.64, No.5, pp.3537–3547 (2017)
- (29) X. Sun, Y. Tang, X. Xiao, and Y. Xie: “Predictive trajectory control strategy for permanent magnet synchronous motor drives based on deadbeat predictive flux linkage control method”, *IEEE Trans. Power Electron.*, Vol.38, No.2, pp.2327–2338 (2023)
- (30) H.-C. Moon, J.-S. Lee, and K.-B. Lee: “A robust deadbeat finite set model predictive current control based on discrete space vector modulation for a grid-connected voltage source inverter”, *IEEE Trans. Energy Convers.*, Vol.33, No.4, pp.1719–1728 (2018)
- (31) J.-H. Lee, J.-S. Lee, H.-C. Moon, and K.-B. Lee: “An improved finite-set model predictive control based on discrete space vector modulation methods for grid-connected three-level voltage source inverter”, *IEEE J. Emerg. Sel. Topics Power Electron.*, Vol.6, No.4, pp.1744–1760 (2018)

Hyung-Woo Lee (Non-member) received his B.S. and M.S. degrees in electrical and computer engineering from Ajou University, Suwon, South Korea, in 2020 and 2022, respectively, where he is currently pursuing a Ph.D. degree. His research interests include dual inverters, electric machine drives, and power conversion.



Jun-Ho Hwang (Non-member) received his B.S. degree in electrical engineering from Myongji University, Yongin, South Korea, in 2021, and the M.S. degree in electrical and computer engineering from Ajou University, Suwon, South Korea in 2023. Since 2023, he has been with the LG Electronics, Seoul, South Korea. His current research interests include electric machine drives, and power conversion systems.



Kyo-Beum Lee (Non-member) received the B.S. and M.S. degrees in electrical and electronic engineering from the Ajou University, Suwon, South Korea, in 1997 and 1999, respectively. He received the Ph.D. degree in electrical engineering from the Korea University, Seoul, South Korea, in 2003. From 2003 to 2006, he was with the Institute of Energy Technology, Aalborg University, Aalborg, Denmark. From 2006 to 2007, he was with the Division of Electronics and Information Engineering, Jeonbuk National University, Jeonju, South Korea. In 2007, he joined the Department of Electrical and Computer Engineering, Ajou University, Suwon, South Korea. He is an Editor-in-Chief of the Journal of Power Electronics. He is an associated editor of the IEEE Transactions on Power Electronics. His research interests include electric machine drives, renewable power generations, and electric vehicle applications.

